CHAPTER 2

Monitoring Intracellular Ca^{2+} in Brain Slices with Fluorescent Indicators

Sean J. Mulligan and Brian A. MacVicar

Introduction

Imaging fluorescent chemical indicators specific for calcium (Ca^{2+}) has provided important insights into our current understanding of the many Ca^{2+} regulated cellular processes in the brain such as neurotransmitter release and synaptic plasticity. In this chapter we discuss the use of fluorescent Ca^{2+} indicators for the measurement of intracellular concentrations ($[Ca^{2+}]_i$) in brain slices. Single-wavelength intensity-modulating indicators are contrasted with dual-wavelength ratiometric indicators and high versus low-affinity indicators are described. The advantages and disadvantages of using a particular indicator form (free acid, AM-ester or dextran conjugate) for reliable Ca^{2+} imaging are outlined. Finally, we review calibration methods to estimate intracellular $[Ca^{2+}]$ from both nonratiometric and ratiometric indicators. This chapter should provide a guide to how and when to use various Ca^{2+} sensitive fluorescent indicators to map the spatio-temporal dynamics of intracellular $[Ca^{2+}]$ in brain slices.

Ca^{2+} Sensitive Fluorescent Chemical Indicators

Our current understanding of the numerous Ca^{2+} regulated physiological cellular phenomena in the brain has been greatly facilitated by the use of the Ca^{2+} sensitive fluorescent chemical probes developed by Tsien and colleagues.[1-10] The most widely used fluorescent indicators for intracellular measurement of free Ca^{2+} concentration ($[Ca^{2+}]_i$) are based on the Ca^{2+} chelator 1,2-bis-(2-aminophenoxy)ethane-*N,N,N',N'*-tetraacetic acid (BAPTA) (Fig. 1). BAPTA has high selectivity for Ca^{2+} ($K_d \approx 100nM$ at pH 7.0) over competing concentrations of Mg^{2+} and an extremely fast on rate (10^8-$10^9 M^{-1}S^{-1}$) for Ca^{2+} binding. The main Ca^{2+} sensitive fluorescent indicators are obtained by coupling different fluorophores with varying spectral properties to the Ca^{2+} sensor BAPTA. The binding of Ca^{2+} to these Ca^{2+} sensitive indicators alters the excitation or emission spectra such that the fluorescence of the indicator that binds the Ca^{2+} can be easily distinguished from the fluorescence of the indicator that remains Ca^{2+} free. The most useful fluorescent probes are those with large molar extinction coefficients and quantum yields that exhibit strong and stable fluorescence well above any background tissue autofluorescence. The wide range of Ca^{2+} sensitive indicators now available (www.probes.com) can be divided into several operational classes based on a number of criteria, the advantages and disadvantages of which should be considered when selecting a probe for a particular experiment; 1) single-wavelength intensity-modulating probes vs. dual-wavelength ratiometric probes, 2) Ca^{2+} binding affinity, and 3) indicator form (salt, AM ester or dextran conjugate).

Voltage-Gated Calcium Channels, edited by Gerald Zamponi.

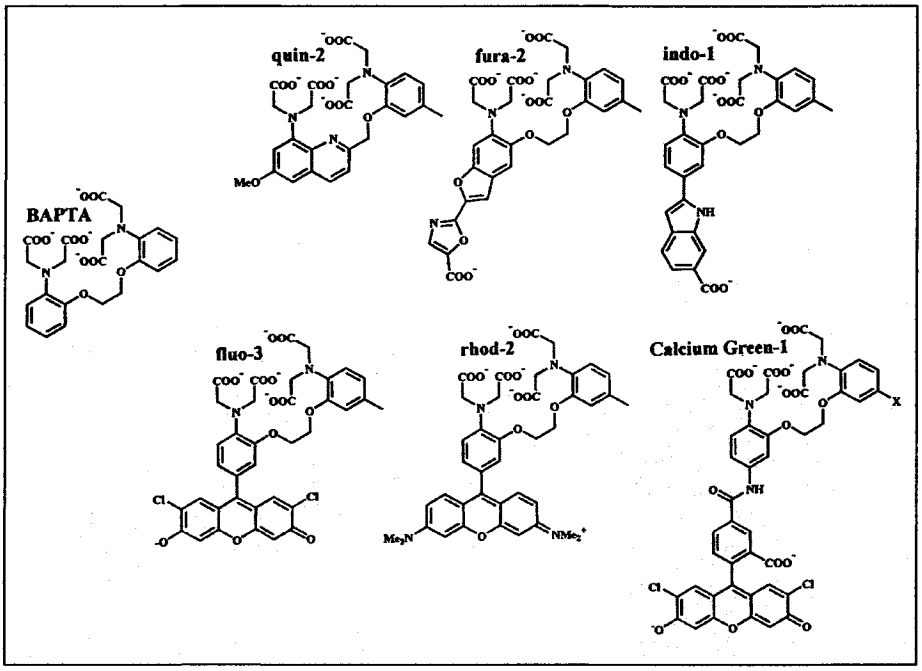

Figure 1. Chemical structures of the Ca^{2+} chelator BAPTA and the widely used BAPTA based fluorescent indicators quin-2, fura-2, indo-1, fluo-3, rhod-2, and Calcium Green-1. Adapted with permission from Tsien RY. Monitoring Cell Calcium. In: Carafoli E, Klee C, eds. Calcium as a Cellular Regulator. New York: Oxford University Press, 1999:28-54.

Single-Wavelength Probes

Increases in $[Ca^{2+}]_i$ result in dramatic increases in the quantum yield of single wavelength probes and hence the intensity of fluorescence emission, while the spectral maxima remain unchanged (i.e., no spectral shift). Fluo-3, rhod-2, and Calcium Green-1 and Calcium Green-2 are examples of commonly used single wavelength Ca^{2+} sensitive indicators that undergo an ~100-fold increase in fluorescence emission upon binding Ca^{2+}[11] (Fig. 2). The high quantum yields characteristic of these single wavelength indicators, serves two important functions when attempting to image $[Ca^{2+}]_i$ in the fine structures associated with neurons and glial cells in brain slices. First, because all Ca^{2+} indicators bind Ca^{2+}, they act as additional buffers in the cell and can significantly alter Ca^{2+} dynamics.[12] In an attempt to measure undistorted changes in $[Ca^{2+}]_i$ it is necessary to balance the relatively low indicator concentrations needed to best report unaltered dynamics of free $[Ca^{2+}]_i$ with the need for sufficient fluorescence intensity that is gained with higher indicator concentrations. The high quantum yield of these indicators permits the use of lower dye concentrations to best report $[Ca^{2+}]_i$ dynamics while at the same time still achieving the necessary signal-to-noise for quantitative measurement. Secondly, laser intensity can be attenuated. The benefit of this is several-fold. First, fluorophores in the excited state are more prone to chemical reactions with other molecules and other fluorophores that can result in irreversible destruction or photobleaching, the final product being nonfluorescent.[13] With laser attenuation, the lifetime of the fluorophore is prolonged. Secondly, fluorophores may not only undergo complete destruction and become nonfluorescent from photodamage, but may remain fluorescent, however unable to report Ca^{2+} changes. For example, basal fluorescence in the apical dendrites of neocortical neurons has been shown to increase linearly with

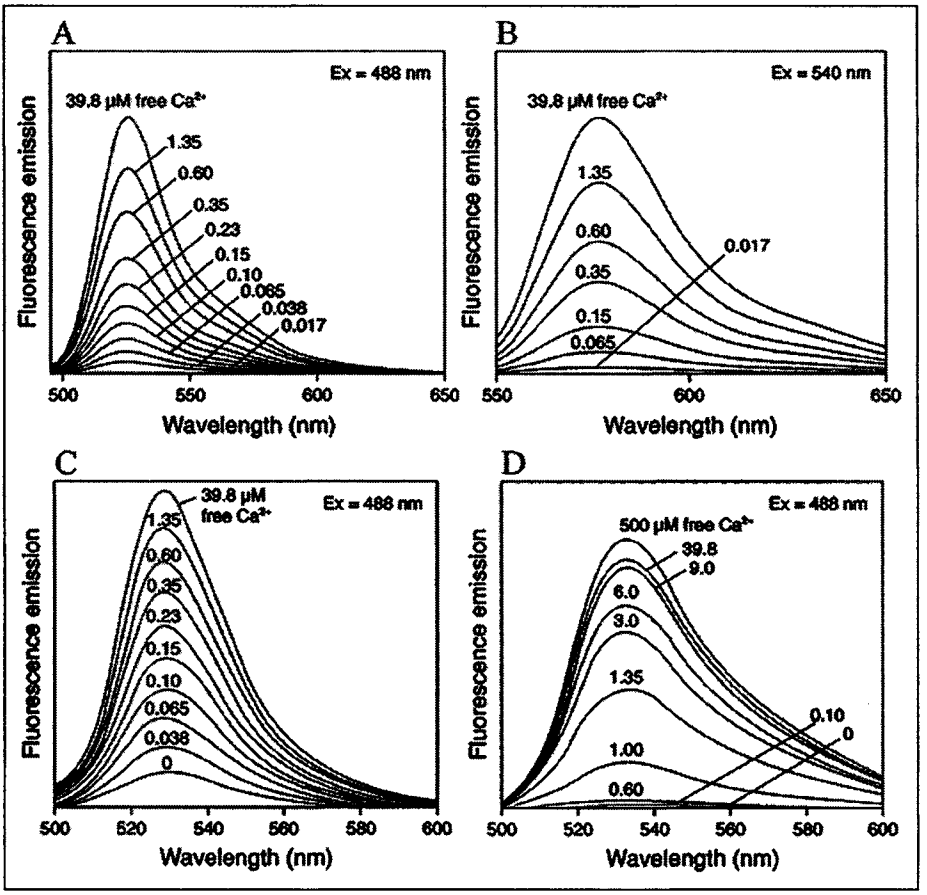

Figure 2. The Ca^{2+}-dependent fluorescence emission spectra of the single wavelength Ca^{2+} sensitive indicators fluo-3 (A), rhod-2(B), Calcium Green-1(C), and Calcium Green-2(D). These indicators are excited by visible wavelengths of light and undergo dramatic increases in the intensity of fluorescence emission upon binding Ca^{2+} with no spectral shift. Adapted with permission from Molecular Probes.[11]

cumulative photodamage.[14] The increased basal fluorescence is thought to result from irreversible photo-induced changes in the fluorophores that bind them to the cellular matrix or membranes. The bound fluorophore is molecularly altered and no longer able to report changes but remains fluorescent. Further, laser attenuation increases cell viability by decreasing phototoxic effects to the cell, independent of photodamage to the fluorophore.

An important characteristic of single wavelength Ca^{2+} sensitive indicators is that they are excited by visible wavelengths of light. This makes this class of indicators well-matched for laser scanning microscopy because they are compatible with the standard fluorescein and rhodamine optical filter configurations common to most imaging system set-ups and they do not require the specialized chromatically corrected optical components necessary for use with UV excitation.[15] Most laser-based systems are supplied with visible excitation lasers that are ideal for efficient excitation. The most common being the 488nm argon-ion laser that is optimal for excitation of the popular indicators fluo-3, Ca^{2+} Green-1, Ca^{2+} Green-2 and Oregon Green 488 BAPTA, and the 543 nm helium/neon-ion laser that is well suited to the excitation maxima of the common red-shifted wavelength probes rhod-2 and Ca^{2+} orange. In addition, visible wavelength light is

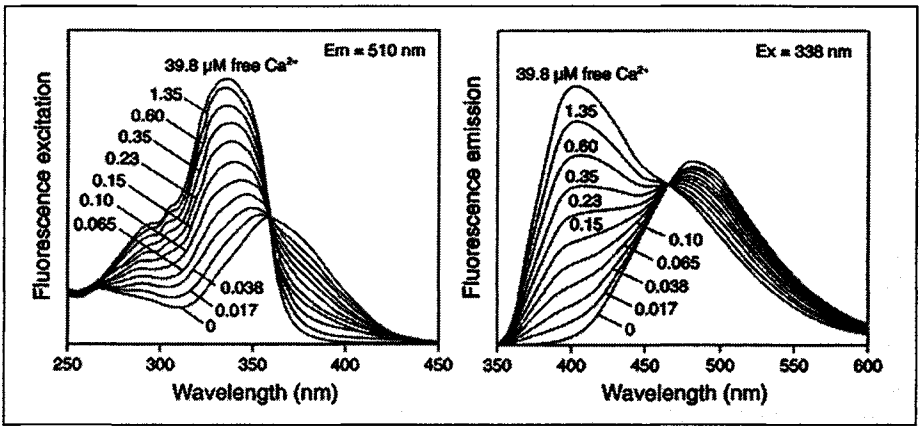

Figure 3. The Ca^{2+}-dependent fluorescence excitation spectra of fura-2 (left) and the emission spectra of indo-1 (right). Both of these common dual-wavelength ratiometric indicators are excited by UV wavelength light and show fluorescence intensity changes and spectral shifts in their excitation spectra (fura-2) or emission spectra (indo-1) with changing $[Ca^{2+}]$. Adapted with permission from Molecular Probes.[11]

less cytotoxic than that of UV excitation[16] and minimizes background scattering and the contribution of tissue autofluorescence, because in mammalian cells, intrinsic fluorescence is dominated by proteins and reduced nucleotides that exhibit strong fluorescence after ultraviolet (UV) excitation (for ex; NADH, NADPH; absorption maximum, 340nm; emission maximum, 460nm).[13] Finally, visible wavelength excited indicators are compatible with photolabile 'caged' Ca^{2+} chelators used for rapidly changing $[Ca^{2+}]_i$ that require UV (~350nm) excitation.[15,17,18]

Dual-Wavelength Ratiometric Probes

Like the single-wavelength probes, the ratiometric probes also show fluorescence intensity changes with changing $[Ca^{2+}]$. Unlike the single-wavelength probes however, the spectral maxima of the Ca^{2+} -free and the Ca^{2+} -bound forms of the ratiometric probes are at different wavelength locations (i.e.; they exhibit a spectral shift). The two most commonly used ratiometric indicators are fura-2 and indo-1.[1] Both these indicators are excited by UV wavelength light with resultant emission in the visible spectrum. They display Ca^{2+} dependent spectral shifts in either their excitation spectra in the case of fura-2, or emission spectra in the case of indo-1 (Fig. 3). The Ca^{2+} -free form of fura-2 displays high fluorescence emission intensity (collected at ~510 nm) when excited by 380nm wavelength light and low emission intensity upon binding Ca^{2+}. Reciprocal changes occur in fluorescence emission intensity when fura-2 is excited at 340nm wavelength light (i.e.; fluorescence emission intensity is low in the Ca^{2+} -free form and highest upon binding Ca^{2+}). In contrast, indo-1 is excited at a single wavelength of light (~340 nm) and the fluorescence intensity monitored at two emission wavelengths. The emission spectral maxima of indo-1 shifts from ~480 nm in the Ca^{2+}-free form to ~400 nm when the indicator is saturated with Ca^{2+}.

Because this class of indicators exhibit Ca^{2+} dependent spectral shifts, fluorescence intensity measurements can be made at two different wavelengths of the spectrum and a ratio calculated to determine $[Ca^{2+}]_i$ (see below). The ratiometric measurements are independent of the fluorescence intensity changes that arise from confounding factors unrelated to changes in $[Ca^{2+}]_i$ such as variations in indicator concentration, cell thickness, focal plane, cell volume or movement, and photobleaching effects to the probe. This fact makes the ratiometric indicators powerful tools for monitoring and quantifying Intracellular $[Ca^{2+}]$. Ratiometric imaging of $[Ca^{2+}]_i$ in brain slices using fura-2 has greatly increased our understanding of the spatio-temporal dynamics of $[Ca^{2+}]_i$ in fine neuronal structures such as dendrites[19-24] and presynaptic terminals.[25-30]

Table 1. Properties of commonly used high- and low-affinity Ca^{2+} indicators

Indicator	Ca^{2+} Free Excitation	Ca^{2+} Free Emisson	Ca^{2+} Bound Excitation	Ca^{2+} Bound Emisson	K_D μM
High-Affinity Indicators					
Fluo-3	503		506	526	0.39
Ca^{2+} Green-1	506	531	506	531	0.19
Ca^{2+} Green-2	506	536	503	536	0.55
Oregon Green 488 BAPTA-1	494	523	494	523	0.17
Rhod-2	548		552	578	0.57
Ca^{2+} Orange	549	575	549	576	0.185
Fura-2	363	512	335	505	0.145
Indo-1	346	475	330	401	0.23
Low-Affinity Indicators					
Mag-Fura-2	369	511	329	508	25
BTC	464	533	401	529	7
Mag Fura-5	369	505	330	500	28
Magnesium Green	506	531	506	531	6
Ca Green-5N	506	532	506	532	14

Ca^{2+} Binding Affinity

Fluorescent Ca^{2+} indicators bind Ca^{2+} in a reversible manner and as a result act as Ca^{2+} buffers once introduced into cells. These exogenous buffers can significantly alter Ca^{2+} dynamics.[12,27,28,31-34] In order to reduce the buffering effects on Ca^{2+} signals, an important criterion for selecting an indicator is matching the Ca^{2+} binding affinity of the indicator to the range of interest over which $[Ca^{2+}]_i$ changes occur during a particular experiment. Ca^{2+} concentrations in astrocytes have been shown to be elevated to 3.5 μM with dopamine application[35] and estimates of Ca^{2+} concentrations exceeding 200 μM have been reported at the inner membrane surface next to voltage-gated Ca^{2+} channel clusters (Ca^{2+} microdomains) in the presynaptic terminals of neurons during stimulation.[36] The common Ca^{2+} indicators mentioned above belong to the high-affinity class of fluorescent Ca^{2+} indicators, having K_D's in the nanamolar range (Table 1). These high-affinity indicators greatly underestimate the increases in $[Ca^{2+}]_i$ during 'physiological' stimulation typically seen in neurons and astrocytes because Ca^{2+} concentrations above 1 μM produce almost complete binding saturation.[11] For example, in the apical dendrites of neocortical layer V and hippocampal CA1 pyramidal neurons in rat brain slices, the amplitude of a single action potential evoked fluorescence transient was reduced by a factor of about three with just 125μM Fura-2.[12] The situation is equally dramatic at the presynaptic terminal. During trains of action potential evoked $[Ca^{2+}]_i$ increases, the fluorescence changes per spike decreased markedly during the train using high-affinity indicators such as Fura-2 and Calcium-Green-2[27,28,33] (Fig. 4 top). The $[Ca^{2+}]_i$ increases during the train saturate the responses of the indicators and thus the fluorescence transient is not linearly related to the changes in $[Ca^{2+}]_i$ and accurate quantification is not possible (given that an equal amount of Ca^{2+} enters the presynaptic terminal with each stimulus in the train (300 nM;).[27]

Low-affinity Ca^{2+} indicators have been developed that have greatly improved our ability to more accurately follow and quantify the activity evoked $[Ca^{2+}]_i$ changes in neurons and astrocytes in brain slice preparations. Mag-fura-2,[37] mag fura-5,[38] BTC,[39] Magnesium Green,[11] and Calcium-Greeen-5N[40] are some of the most widely used low-affinity Ca^{2+} indicators that can detect $[Ca^{2+}]_i$ levels in the micromolar range (Table 1). The spectral shifts of the Fura-2

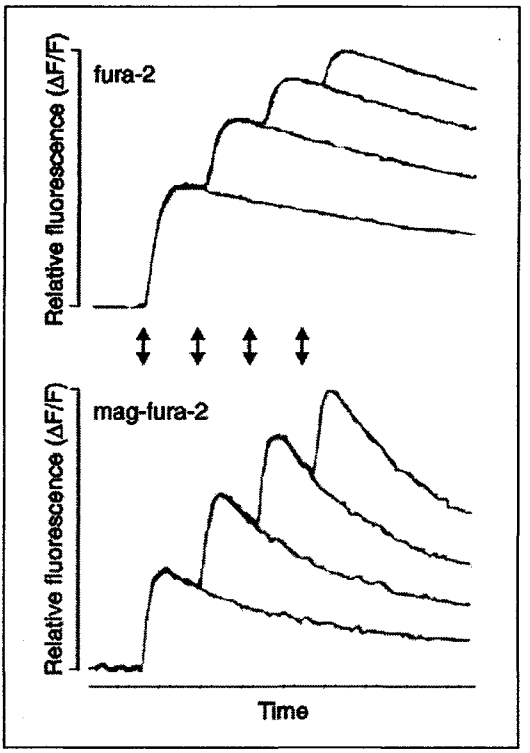

Figure 4. High-affinity Ca^{2+} indicators distort rapid Ca^{2+} changes. During trains of action potential evoked $[Ca^{2+}]_i$ increases (20Hz stimulus pulses indicated by double-arrows), the fluorescence changes per spike decrease markedly due to saturation of the high-affinity indicator Fura-2. The $[Ca^{2+}]_i$ increases do not saturate the response when the low-affinity indicator mag-fura-2 is used. Each stimulus in the train produces approximately the same change in fluorescence and thus the fluorescence transient is linearly related to the changes in $[Ca^{2+}]_i$. In addition, the decay time course of the Ca^{2+} transients using the low-affinity indicator mag-fura-2 is undistorted. Reprinted with permission from Molecular Probes[11] and Regehr WG, Atluri PP, Calcium transients in cerebellar granule cell presynaptic terminals. Biophys J 1995; 68(5):2156-70.

analogs mag-fura-2 and mag-fura-5 are very similar to those of fura-2 but occur at higher Ca^{2+} concentrations (K_D's $\approx$ 25 μM and 28 μM respectively). BTC exhibits a shift in excitation maximum from ~480 nm to ~400 nm upon binding Ca^{2+} which makes it the only low-affinity ratiometric indicator ($K_d \approx 7$ μM) with visible excitation wavelengths. BTC thus permits ratiometric measurements of $[Ca^{2+}]_i$ while retaining the advantages associated with using longer wavelength excitation (outlined above). The spectral properties of the single-wavelength low-affinity Calcium-Green analoges Calcium Green-5N and Magnesium Green are the same as Calcium Green-1 but have K_D's $\approx$ 14 μM and 6 μM respectively.

In addition to underestimating increases in $[Ca^{2+}]_i$, high-affinity Ca^{2+} indicators significantly distort the kinetics of rapid Ca^{2+} changes associated with the physiological processes that operate on millisecond time scales in neurons and astrocytes. Both the high- and low-affinity classes of fluorescent indicators have Ca^{2+} binding on-rates in the range of 10^8-$10^9 M^{-1}s^{-1}$. They differ significantly however with respect to their off-rates. Low-affinity indicators have much faster Ca^{2+} dissociation rates that make them much more suitable for tracking the kinetics of rapid Ca^{2+} fluxes (the backward rate constants (k-) for Fura-2 and Mag-Fura2 are ~$100s^{-1}$ and $26{,}000s^{-1}$ respectively). For example, the decay time constants of fluorescent transients evoked

by single back-propagating action potentials in the apical dendrites of neocortical and hippocampal CA1 neurons increased dramatically with increasing concentrations of the high-affinity indicator Fura-2.[12,41] Fura-2 concentrations of 20, 80 125, and 250 μM corresponded to decay time constants of 78, 117, 265 and 703 msec respectively.[12] In contrast, in a study with parallel experimental procedures, high concentrations (up to 2mM) of the low-affinity indicators Magnesium Green and Oregon green BAPTA-5N did not distort the decay time course of action potential evoked $[Ca^{2+}]_i$ transients, but in fact, were faster than the predicted 'physiological' $[Ca^{2+}]_i$ transient (estimated from linear regression extrapolation to zero fura-2, during Fura-2 concentration dependence of decay time constant experiments).[24] At the presynaptic terminal the properties of the fluorescent transients also depend on the affinity of the indicator used. As discussed above, during trains of action potential evoked $[Ca^{2+}]_i$ increases, the fluorescence changes per spike decrease markedly during the trains using high-affinity indicators such as fura-2 and Calcium-Green-2 (Fig. 4 top). However, the $[Ca^{2+}]_i$ increases during trains did not saturate the response when low-affinity indicators were used. Each stimulus in the train produced approximately the same change in fluorescence and thus the fluorescence transient is linearly related to the changes in $[Ca^{2+}]_i$ and accurate quantification is possible.[27,28,33] (Fig. 4 bottom) The slow Ca^{2+} binding off-rates of the high-affinity indicators make them unable to reliably track the decay time course of the Ca^{2+} transients in presynaptic terminals[27,28,33,42] (Fig. 4 for qualitative decay comparison). At climbing fiber presynaptic terminals, single action potential evoked Calcium Green fluorescent transients decayed with a half decay time of 168 msec compared to only 33 msec with the novel low-affinity indicator Fluo-4 Dextran.[43]

Ca^{2+} Indicator Form

Salts (Free Acids)

The common salt (or free acid) form of the Ca^{2+} indicators are negatively charged polycarboxylate anions that are membrane impermeant and so must be introduced into cells by microinjection. Because this form of the indicator is negatively charged, cells may be filled by iontophoretic injection using high resistance sharp electrodes (50-150 MΩ) that contain millimolar indicator concentrations.[22,44,45] Cells are rapidly filled with indicator using this technique while the intracellular environment is not dialyzed with pipette solutions (hyperpolarizing at -0.2-0.5nA for 2-5 minutes loads an entire neocortical pyramidal cell with indicator).[46] Patch-clamping neurons and astrocytes in brain slices in the whole-cell configuration[47] with low resistance pipettes (3-10 MΩ) has become the preferred method for loading impermeant indicators into cells and simultaneously making electrophysiological measurements. Micromolar concentrations of indicator (50-500 μM) are loaded by the rapid diffusional exchange that takes place between the low resistance pipette tip and the intracellular cytoplasm.[48] This allows for defined intracellular indicator concentrations to be determined, which is a critical parameter in indicator calibrations (see below). The great advantage of using the free acid indicator form (in addition to avoiding the problems associated with using the AM-ester form -see below) is the remarkable fluorescence signal-to-noise achieved. Images from the finest neuronal structures are possible, including individual dendritic spines, axons and presynaptic terminals, and the Ca^{2+} transients in these structures can be reliably quantified (Fig. 5A,B).[29,30,49-53]

Dextran Conjugates

Fluorescent Ca^{2+} indicators may be conjugated to dextrans, which are 3000 to 500,000 MW biologically inert hydrophilic polysaccharides. As with the salt forms, dextran conjugates are not membrane permeable and so must gain intracellular access by whole-cell patch pipette. Iontophoretic injection is not suitable because there is a reduction in the negative charge per unit mass. While the spectral characteristics of the dextran conjugates are similar to the free acid forms, the Ca^{2+} binding affinity is slightly reduced. For example, the K_D of the salt form of Fura-2 is 145 nM compared to 200-400 nM for Fura-2 dextran.[11] Molecular probes (Eugene,

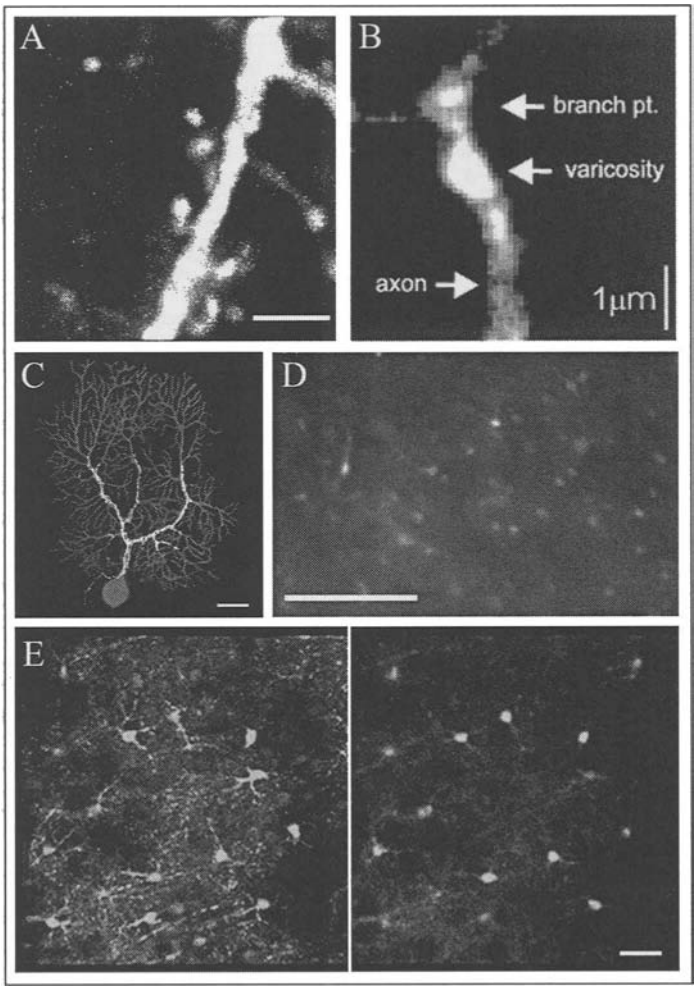

Figure 5. Neurons and astrocytes in the brain slice preparation loaded with the free acid, dextran conjugate, or AM-ester forms of Ca^{2+} sensitive indicators. A) Two-photon image of a pyramidal neuron dendrite with spines from mouse visual cortex filled with 200 μM of the free acid form of Calcium Green-1 by whole cell patch pipette. (scale=5 μm) Reprinted with permission from Holthoff K, Tsay D, Yuste R. Calcium dynamics of spines depend on their dendritic location. Neuron. 2002 Jan 31;33(3):425-37. B) Two-photon image of an axonal arbor of a layer 2/3 neocortical pyramidal neuron filled with 100 μM of the free acid form of Oregon BAPTA-1 via patch pipette. (scale=1 μm) Reprinted with permission from Cox CL, Denk W, Tank DW, Svoboda K. Action potentials reliably invade axonal arbors of rat neocortical neurons. Proc Natl Acad Sci U S A 2000; 97(17):9724-8. C) An overlay of two confocal image stacks in a sagital cerebellar slice showing a Calcium Green Dextran-labeled climbing fiber incoming axon (white) innervating the thick proximal dendrites of a Purkinje neuron (grey) labeled with the fluorescent dye Alexa Fluor 568 hydrazide (Molecular Probes). (scale=20 μm) Reprinted with permission from Kreitzer AC, Gee KR, Archer EA, Regehr WG. Monitoring presynaptic calcium dynamics in projection fibers by in vivo loading of a novel calcium indicator. Neuron. 2000; 27(1):25-32. D) Dozens of neurons in layer 2/3 somatosensory cortex are labeled with the AM-ester form of Fura-2. The brain slice was taken from an 18 day old rat. (scale=100 μm) Reprinted with permission from Smetters D, Majewska A, Yuste R. Detecting action potentials in neuronal populations with calcium imaging. Methods. 1999;18(2):215-21. E) Two-photon image stack f GFP labeled astrocytes (left) loaded with Ca^{2+} Orange-AM (right). (scale=20 μm). Mulligan and MacVicor unpublished observations.

OR) offers a 70,00MW dextran simultaneously conjugated to Calcium Green-1 and the Ca^{2+}-insensitive dye Texas Red that provides ratiometric Ca^{2+} measurements with visible wavelength excitation. Dextran-conjugated Ca^{2+} indicators retain all the advantages the salt form indicators have over AM-ester forms, and in addition, are much less likely to bind to cellular proteins and are better retained in cells and less resistant to extrusion.[11] The fact that they do not leak out of cells makes them ideally suited for long-term Ca^{2+} measurements and excellent retrograde and anterograde tracers.[54,55] Krietzer et al (2000)[43] have loaded dextrans in to the cellular nuclei of the inferior olive in vivo, and monitored Ca^{2+} dynamics days later in presynaptic terminals at the cerebellar climbing fiber to Purkinje cell synapse (Fig. 5C).

AM-Esters

Loading neurons and astrocytes in brain slices can be achieved without the use of micropipettes for indicator injection and disruption to cell membranes. The negative charged carboxylate groups of the salt and dextran-conjugated forms of Ca^{2+} indicators that render them hydrophilic and cell impermeant, may be derivatized as acetoxymethyl (AM) –esters.[5] The AM-ester form of the Ca^{2+} indicator is lipophilic, membrane-permeant and insensitive to ions. Incubation of brain slices in a solution of the AM-ester form results in cellular loading by diffusion through the cell membrane. Once inside the cells, the acetyl-ester linkages are then hydrolyzed by intracellular esterases to release the active Ca^{2+} sensitive indicator, which is now membrane-impermeant and trapped in the cytoplasm.

The advantage of using the AM-ester form of indicator, is that it facilitates the bulk loading of many cells or many specific cellular structures, while avoiding delicate intracellular microelectrode techniques required for loading the salt and dextran-conjugate forms. This method then, provides a way of monitoring intracellular Ca^{2+} dynamics in many neurons (or neuronal processes) and astrocytes in a brain slice. For example, Yuste and colleagues have been able to bulk load AM-ester forms of Ca^{2+} indicators into populations of neurons in brain slices and image somatic Ca^{2+} transients (Fig. 5D).[56-58] By stimulating one excitatory neuron while imaging hundreds of others they are able to identify connected neurons and begin to explore cortical microcircuitry. Regehr and Tank (1991)[59] developed a method for selectively filling presynaptic terminals in adult brain slices by localized perfusion with the AM-ester form of Fura-2. They and others have used this method to image presynaptic Ca^{2+} transients and have greatly contributed to our current understanding of the role of Ca^{2+} in synaptic transmission at central synapses.[26-28,42,60-67] Astrocytes in brain slices are readily loaded with AM-esters (Fig. 5E). Results from studies monitoring Ca^{2+} transients in AM-ester loaded astrocytes has forced us to expand our current view of the functional roles astrocytes play in theø central nervous system. For example, it is now believed that astrocytes are involved in activity-dependent modulation of synaptic transmission and that spontaneous intrinsic Ca^{2+} oscillations in astrocytes can propagate and act as a primary source for generating neuronal activity.[68,69]

There are a number of pitfalls of using AM-ester Ca^{2+} indicators. First and foremost there is a dramatic reduction in the cellular fluorescence signal-to-noise over background compared with the intracellular injected forms due to nonspecific loading and indicator that remains extracellular but fluorescent. Another major problem is incomplete hydrolysis of the esters. The fully esterfied form of Fura-2 for example contains five AM groups linked to the carboxylate groups.[11] If there is not complete hydrolysis of all five groups a new form that is Ca^{2+} insensitive yet highly fluorescent remains.[70] Incomplete hydrolysis can also result in sequestering or compartmentalization inside the cell.[71,72] If the cell has low esterase activity and slow de-esterification results, the indicator is able to move freely from the cytoplasm and into intracellular organelles such as mitochondria, sarcoplamic reticulum, lysosomes and the nucleus where it then becomes cleaved and remains trapped there but unable to report cytoplasmic Ca^{2+} changes.[73] Extrusion across the plasma membrane by the multidrug resistance transporter is also a problem that is specific to the AM form but not the free acid or dextran forms.[74] The above problems make it virtually impossible to perform quantitative indicator calibrations in

vivo (see below). A final complication of the AM-ester form is that the successful loading of neurons is highly age dependent. Indeed, few labs have been able to load any neurons in adult brain slices (but esee ref. 56).

Quantitative Measurement of $[Ca^{2+}]_i$

Ratiometric Calibration

The best quantitative descriptions of $[Ca^{2+}]_i$ can be achieved when using dual-wavelength ratiometric dyes, such as fura-2, because fluorescence measurements can be made at two different wavelengths and a ratio calculated to determine $[Ca^{2+}]_i$ independent of the fluorescence intensity changes that arise from confounding factors unrelated to changes in $[Ca^{2+}]_i$, such as variations in indicator concentration, cell thickness, focal plane, cell volume or movement, photobleaching effects to the probe, and instrument sensitivity. The relationship between $[Ca^{2+}]_i$ and the experimentally measured fluorescence is described in the calibration equation given by Grynkiewicz et al (1985);

$$[Ca^{2+}]_i = K_D\ (R\text{-}R_{min}/R_{max}\text{-}R)\ (S_{f2}/S_{b2})$$

For Fura-2, K_D is the dissociation constant of Fura-2, R is the background corrected experimentally measured ratio of fluorescence intensity produced by 340 nm and 380 nm excitation, R_{min} is the ratio at 0 $[Ca^{2+}]_i$, R_{max} is the ratio at a saturating $[Ca^{2+}]$, and S_{f2}/S_{b2} is the ratio of the fluorescence intensities in 0 $[Ca^{2+}]$ and saturating $[Ca^{2+}]$. To determine R_{min}, R_{max}, and S_{f2}/S_{b2}, in vitro or in vivo calibrations must be performed and requires that the K_D for the indicator be known. These calibrations entail using a set of buffer solutions of known $[Ca^{2+}]$, and are available in 'Kit' form from Molecular Probes. When doing calibrations, it is again important to consider the Ca^{2+} binding affinity of the indicator. Kits for high-affinity Ca^{2+} indicators contain 10 mM K_2EGTA and 10 mM CaEGTA buffered solutions that provide a range of "zero" free Ca^{2+} to 40 μM free Ca^{2+}. Solutions for low-Affinity Ca^{2+} Indicator calibration provide a range from 1 μM to 1 mM free Ca^{2+}. The choice of whether to do an in vitro or in vivo calibration will depend on the indicator loading technique used during the experiment, i.e.; bulk loading with AM-esters or whole-cell patch pipette.

AM ester-loading indicators require calibrations to be performed in vitro, under conditions that closely mimic experimental conditions. Incomplete hydrolysis of the AM-ester, indicator compartmentalization, and ineffective access of ionophores (used to equilibrate $[Ca^{2+}]_i$ with buffers of known Ca^{2+} concentrations) into regions within brain slices, as well as indicator leakage from the cells when permeabilized all make in vivo calibration impractical.[26,11] In vitro calibrations suffer however, from the fact that the spectral properties of the indicator are altered by the pH, ionic strength, intracellular binding and uptake and viscosity of the cytoplasmic environment and thus do not represent in vivo conditions.[72,75] In an attempt to correct viscosity, a viscosity correction (0.7-0.85) may be applied.[76] In vivo calibrations are possible when indicator loading with whole-cell patch pipettes because the pipette has direct access to the intracellular environment and thus circumvents the problems associated with using ionophores for the equilibration of internal and external $[Ca^{2+}]$.[48] During these calibrations, standard intracellular patch solutions are loaded to different known $[Ca^{2+}]$ levels, the fluorescence ratios experimentally measured and the parameters R_{min}, R_{max}, and S_{f2}/S_{b2} determined.

Single-Wavelength Calibration

Single-wavelength indicators are fluorescence intensity modulating probes and so do not allow for wavelength ratioing. As an alternative, when imaging $[Ca^{2+}]_i$ in neurons and astrocytes in brain slices it is typical to report $[Ca^{2+}]_i$ changes in normalized terms of relative florescence changes over the baseline fluorescence level, commonly known as $\Delta F/F$.[51,50,69,77-80]

Defined as;

$$\Delta F/F = ((F_1 - B_1) - (F_0 - B_0))/(F_0 - B_0)$$

where F_1 and F_0 are fluorescence in the imaged region of interest at any given time point and at the beginning of the experiment respectively, and B_1 and B_0 are the background fluorescence at any given time point and at the beginning of the experiment respectively. Background values are taken from an adjacent area distant to any indicator-containing structures. Although reporting $[Ca^{2+}]_i$ changes in terms of $\Delta F/F$ does not allow for quantitative molar measurement of $[Ca^{2+}]_i$, it is independent of indicator concentration, optical path and imaging sensitivity and is useful for reporting relative changes, induced for example by drug application. To accurately assess relative $[Ca^{2+}]_i$ changes however, it is necessary to show that the fluorescent transients are linearly related to the changes in $[Ca^{2+}]_i$. This condition is best met by using low-affinity indicators, as saturation of high-affinity indicators occurs during most physiological increases in $[Ca^{2+}]_i$ at typical indicator concentrations used and results in nonlinear changes.[12,27,28,51,56,81,82]

In theory, fluorescence signals from single wavelength indicators can be converted to $[Ca^{2+}]_i$ by the equation given by Grynkiewicz et al (1985);

$$[Ca^{2+}]_i = K_D (F-F_{min}/F_{max}-F)$$

where K_D is the dissociation constant of the indicator, F is the background subtracted experimentally measured fluorescence intensity, F_{min} is the fluorescence intensity at 0 $[Ca^{2+}]_i$, and F_{max} is the fluorescence intensity at a saturating a $[Ca^{2+}]$. Analogous to the situation using ratiometric indicators, the indicator K_D must be known and F_{min} and F_{max} determined from calibrations with solutions of known $[Ca^{2+}]$. F_{min} and F_{max} can only be reliably established in an in vitro setting at the same indicator concentration, optical pathlength and without any photobleaching or change in instrument sensitivity because the great variability in these requirements makes performing in vivo calibrations not practical. Quantitative measurements of intracellular Ca^{2+} concentrations may be determined from single wavelength indicators in vivo however, if coloaded with another indicator of a differing wavelength. For example, because the single-wavelength indicators Fluo-3 and Fura Red exhibit reciprocal shifts in fluorescence intensity upon binding Ca^{2+}, ratiometric measurements of $[Ca^{2+}]_i$ are possible.[83,84] Simply coloading single-wavelength Ca^{2+} indicators with Ca^{2+}-insensitive indicators that are excited at the same wavelengths, but detected at much longer wavelengths can also be done to make ratiometric measurements possible.

Changes in calcium concentration ($\Delta[Ca^{2+}]_i$) can be quantified by two methods with single-wavelength indicators, one method for use with low-affinity Ca^{2+} indicators and the other for use with high-affinity indicators. The method appropriate for use with low-affinity indicators is based on the relative florescence changes over baseline fluorescence levels ($\Delta F/F$). Fluorescence intensity changes can be converted to changes in $[Ca^{2+}]_i$ using the following formula;[85]

$$(\Delta[Ca^{2+}]_i = (K_D / (\Delta F/F)_{max}) (\Delta F/F) (\Delta F/F << (\Delta F/F)_{max})$$

where, the parameters are the same as above and $(\Delta F/F)_{max}$ is the maximal change in fluorescence upon indicator saturation, which can be estimated in neurons using strong stimulation. The formula is only applicable if the indicator is far from saturation during evoked changes in $[Ca^{2+}]_i$, a condition met with low-affinity Ca^{2+} indicators. The method appropriate for use with high-affinity indicators is derived from the nonlinear dependence of fluorescence on $[Ca^{2+}]_i$ caused by high-affinity indicator saturation. Two closely timed stimulation pulses produces fluorescent transients (for example, action potential evoked Ca^{2+} influx into dendritic spines[77] or presynaptic terminals,[55,85] the second of which is smaller than the first when loaded with high-affinity Ca^{2+} indicators but not low-affinity indicators.[27,33,55,77,85] This indicates that partial saturation of the high-affinity indicators is responsible for the $\Delta F/F$ decrements and enable quantification of changes in intracellular Ca^{2+} influx ($\Delta[Ca^{2+}]_i$) per action potential using the following formula;

$$\Delta[Ca^{2+}]_i = ([Ca^{2+}]_0 + K_D) (1 - \alpha) / 2\alpha$$

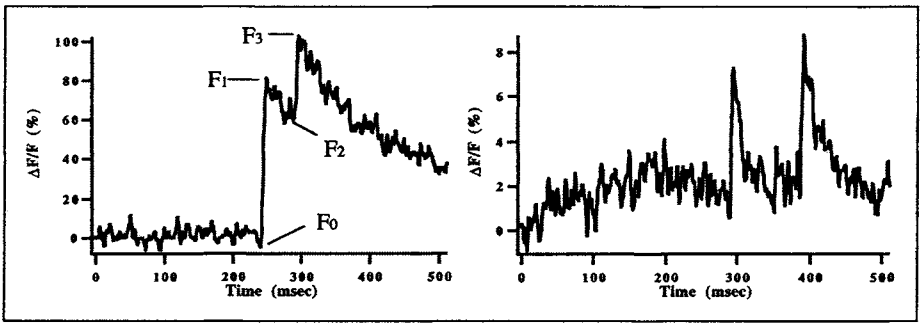

Figure 6. Quantification of changes in intracellular Ca^{2+} influx per action potential is possible using high-affinity indicators. Two closely timed stimulation pulses produces fluorescent transients in a CA1 neuron, the second of which is smaller than the first when loaded with the high-affinity Ca^{2+} indicator Calcium Green-1 (500 μM)(left), but not with the low-affinity indicator Magnesium Green (500 μM)(right). See accompanying text for explanation of symbols. Reprinted with permission from Yuste R, Majewska A, Cash SS, Denk W. Mechanisms of calcium influx into hippocampal spines: heterogeneity among spines, coincidence detection by NMDA receptors, and optical quantal analysis. J Neurosci 1999; 19(6):1976-87.

where $\alpha = (F_3 - F_2) / (F_1 - F_0)$ and $[Ca^{2+}]_0$ is the estimated resting Ca^{2+} concentration, K_D is the dissociation constant of the indicator, F_0 is the indicator fluorescence at resting $[Ca^{2+}]_0$, F_1 is the peak fluorescence produced by the first action potential, F_2 is the fluorescence immediately before the second action potential, and F_3 is the peak fluorescence produced by the second action potential (Fig. 6 left). Use of this equation to estimate $\Delta[Ca^{2+}]_i$ assumes that the influxes produced by each action potential are the same (as confirmed by low affinity indicators (Fig. 6 right)[27,33,55,77,85] and that the decay in $[Ca^{2+}]_i$ between action potentials is small compared with the peak $[Ca^{2+}]_i$.

Conclusion

The use of Ca^{2+} sensitive fluorescent indicators has proven to be an indispensable tool for studying the spatio-temporal dynamics of intracellular $[Ca^{2+}]$, which plays a critical role in many cellular processes. In this chapter we have discussed commonly used fluorescent Ca^{2+} indicators for the measurement of intracellular $[Ca^{2+}]$ in neurons and astrocytes in brain slice preparations. By reviewing the properties of the several operational indicator classes and discussing the experimental advantages and disadvantages of each, it is hoped that many of the experimental pitfalls may be avoided when attempting to accurately follow and quantify intracellular $[Ca^{2+}]$ changes.

References

1. Grynkiewicz G, Poenie M, Tsien RY. A new generation of Ca^{2+} indicators with greatly improved fluorescence properties. J Biol Chem 1985; 260:3440-3450.
2. Minta A, Kao JP, Tsien RY. Fluorescent indicators for cytosolic calcium based on rhodamine and fluorescein chromophores. J Biol Chem 1989; 264:8171-8178.
3. Poenie M, Tsien R. Fura-2: A powerful new tool for measuring and imaging $[Ca^{2+}]$i in single cells. Prog Clin Biol Res 1986; 210:53-56.
4. Tsien RY. New calcium indicators and buffers with high selectivity against magnesium and protons: design, synthesis, and properties of prototype structures. Biochemistry 1980; 19:2396-2404.
5. Tsien RY. A nondisruptive technique for loading calcium buffers and indicators into cells. Nature 1981; 290:527-528.
6. Tsien RY, Pozzan T, Rink TJ. Calcium homeostasis in intact lymphocytes: Cytoplasmic free calcium monitored with a new, intracellularly trapped fluorescent indicator. J Cell Biol 1982; 94:325-334.
7. Tsien RY. Intracellular measurements of ion activities. Annu Rev Biophys Bioeng 1983; 12:91-116.

8. Tsien RY. Measuring and manipulating cytosolic Ca^{2+} with trapped indicators. Kroc Found Ser 1984; 17:147-155.
9. Tsien RY, Rink TJ, Poenie M. Measurement of cytosolic free Ca^{2+} in individual small cells using fluorescence microscopy with dual excitation wavelengths. Cell Calcium 1985; 6:145-157.
10. Tsien RY. Fluorescent indicators of ion concentrations. Methods Cell Biol 1989; 30:127-156.
11. Haugland RP. Handbook of fluorescent probes and research products. In: Oregon E, ed. Molecular Probes, 9th ed. 2002:984 pages.
12. Helmchen F, Imoto K, Sakmann B. Ca^{2+} buffering and action potential-evoked Ca^{2+} signaling in dendrites of pyramidal neurons. Biophys J 1996; 70:1069-1081.
13. Slavik J. Fluorescent probes in cellular and molecular biology. Boca Ratan: CRC Press, 1994.
14. Koester HJ, Baur D, Uhl R et al. Ca^{2+} fluorescence imaging with pico and femtosecond two-photon excitation: signal and photodamage. Biophys J 1999; 77:2226-2236.
15. Niggli E, Piston DW, Kirby MS et al. A confocal laser scanning microscope designed for indicators with ultraviolet excitation wavelengths. Am J Physiol 1994; 266:C303-310.
16. Brakenhoff GJ, Muller M, Ghauharali RI. Analysis of efficiency of two-photon versus single-photon absorption of fluorescence generation in biological objects. J Microsc 1996; 183:140-144.
17. van Koeveringe GA, van Mastrigt R. Photolysis of caged calcium using a low-cost flash unit. Methods Mol Biol 1999; 114:209-220.
18. Parpura V, Haydon PG. "Uncaging" using optical fibers to deliver UV light directly to the sample. Croat Med J 1999; 40:340-345.
19. Regehr WG, Connor JA, Tank DW. Optical imaging of calcium accumulation in hippocampal pyramidal cells during synaptic activation. Nature 1989; 341:533-536.
20. Regehr WG, Tank DW. Postsynaptic NMDA receptor-mediated calcium accumulation in hippocampal CA1 pyramidal cell dendrites. Nature 1990; 345:807-810.
21. Larkum ME, Kaiser KM, Sakmann B. Calcium electrogenesis in distal apical dendrites of layer 5 pyramidal cells at a critical frequency of back-propagating action potentials. Proc Natl Acad Sci USA 1999; 96:14600-14604.
22. Yuste R, Gutnick MJ, Saar D et al. Ca^{2+} accumulations in dendrites of neocortical pyramidal neurons: an apical band and evidence for two functional compartments. Neuron 1994; 13:23-43.
23. Schiller J, Helmchen F, Sakmann B. Spatial profile of dendritic calcium transients evoked by action potentials in rat neocortical pyramidal neurones. J Physiol 1995; 487:583-600.
24. Kaiser KM, Zilberter Y, Sakmann B. Back-propagating action potentials mediate calcium signalling in dendrites of bitufted interneurons in layer 2/3 of rat somatosensory cortex. J Physiol 2001; 535:17-31.
25. Regehr WG, Tank DW. The maintenance of LTP at hippocampal mossy fiber synapses is independent of sustained presynaptic calcium. Neuron 1991; 7:451-459.
26. Regehr WG, Delaney KR, Tank DW. The role of presynaptic calcium in short-term enhancement at the hippocampal mossy fiber synapse. J Neurosci 1994; 14:523-537.
27. Regehr WG, Atluri PP. Calcium transients in cerebellar granule cell presynaptic terminals. Biophys J 1995; 68:2156-2170.
28. Mintz IM, Sabatini BL, Regehr WG. Calcium control of transmitter release at a cerebellar synapse. Neuron 1995; 15:675-688.
29. Wu LG, Borst JG, Sakmann B. R-type Ca^{2+} currents evoke transmitter release at a rat central synapse. Proc Natl Acad Sci USA 1998; 95:4720-4725.
30. Wu LG, Westenbroek RE, Borst JG et al. Calcium channel types with distinct presynaptic localization couple differentially to transmitter release in single calyx-type synapses. J Neurosci 1999; 19:726-736.
31. Eilers J, Callewaert G, Armstrong C et al. Calcium signaling in a narrow somatic submembrane shell during synaptic activity in cerebellar Purkinje neurons. Proc Natl Acad Sci USA 1995; 92:10272-10276.
32. Stout AK, Reynolds IJ. High-affinity calcium indicators underestimate increases in intracellular calcium concentrations associated with excitotoxic glutamate stimulations. Neuroscience 1999; 89:91-100.
33. Sinha SR, Wu LG, Saggau P. Presynaptic calcium dynamics and transmitter release evoked by single action potentials at mammalian central synapses. Biophys J 1997; 72:637-651.
34. Maravall M, Mainen ZF, Sabatini BL et al. Estimating intracellular calcium concentrations and buffering without wavelength ratioing. Biophys J 2000; 78:2655-2667.
35. Parpura V, Haydon PG. Physiological astrocytic calcium levels stimulate glutamate release to modulate adjacent neurons. Proc Natl Acad Sci USA 2000; 97:8629-8634.
36. Simon SM, Llinas RR. Compartmentalization of the submembrane calcium activity during calcium influx and its significance in transmitter release. Biophys J 1985; 48:485-498.

37. Raju B, Murphy E, Levy LA et al. A fluorescent indicator for measuring cytosolic free magnesium. Am J Physiol 1989; 256:C540-548.
38. Illner H, McGuigan JA, Luthi D. Evaluation of mag-fura-5, the new fluorescent indicator for free magnesium measurements. Pflugers Arch 1992; 422:179-184.
39. Iatridou H, Foukaraki E, Kuhn MA et al. The development of a new family of intracellular calcium probes. Cell Calcium 1994; 15:190-198.
40. Rajdev S, Reynolds IJ. Calcium green-5N, a novel fluorescent probe for monitoring high intracellular free Ca^{2+} concentrations associated with glutamate excitotoxicity in cultured rat brain neurons. Neurosci Lett 1993; 162:149-152.
41. Regehr WG, Tank DW. Calcium concentration dynamics produced by synaptic activation of CA1 hippocampal pyramidal cells. J Neurosci 1992; 12:4202-4223.
42. Sabatini BL, Regehr WG. Optical measurement of presynaptic calcium currents. Biophys J 1998; 74:1549-1563.
43. Kreitzer AC, Gee KR, Archer EA et al. Monitoring presynaptic calcium dynamics in projection fibers by in vivo loading of a novel calcium indicator. Neuron 2000; 27:25-32.
44. Helmchen F, Svoboda K, Denk W et al. In vivo dendritic calcium dynamics in deep-layer cortical pyramidal neurons. Nat Neurosci 1999; 2:989-996.
45. Svoboda K, Helmchen F, Denk W et al. Spread of dendritic excitation in layer 2/3 pyramidal neurons in rat barrel cortex in vivo. Nat Neurosci 1999; 2:65-73.
46. Svoboda KT DW, Stepnoski RA, Denk W. Two-photon imaging of neuronal function in the neocortex in vivo. Imaging neurons: A laboratory manual. R. Yuste, F. Lanni, A. Konnerth ed. New York: Cold Spring Harbor Laboratory Press, 2000: 22.1-22.11.
47. Hamill OP, Marty A, Neher E et al. Improved patch-clamp techniques for high-resolution current recording from cells and cell-free membrane patches. Pflugers Arch 1981; 391:85-100.
48. Pusch M, Neher E. Rates of diffusional exchange between small cells and a measuring patch pipette. Pflugers Arch 1988; 411:204-211.
49. Cox CL, Denk W, Tank DW et al. Action potentials reliably invade axonal arbors of rat neocortical neurons. Proc Natl Acad Sci USA 2000; 97:9724-9728.
50. Sabatini BL, Svoboda K. Analysis of calcium channels in single spines using optical fluctuation analysis. Nature 2000; 408:589-593.
51. Koester HJ, Sakmann B. Calcium dynamics in single spines during coincident pre and postsynaptic activity depend on relative timing of back-propagating action potentials and subthreshold excitatory postsynaptic potentials. Proc Natl Acad Sci USA 1998; 95:9596-9601.
52. Schiller J, Schiller Y, Clapham DE. NMDA receptors amplify calcium influx into dendritic spines during associative pre and postsynaptic activation. Nat Neurosci 1998; 1:114-118.
53. Majewska A, Brown E, Ross J et al. Mechanisms of calcium decay kinetics in hippocampal spines: role of spine calcium pumps and calcium diffusion through the spine neck in biochemical compartmentalization. J Neurosci 2000; 20:1722-1734.
54. O'Donovan MJ, Ho S, Sholomenko G et al. Real-time imaging of neurons retrogradely and anterogradely labelled with calcium-sensitive dyes. J Neurosci Methods 1993; 46:91-106.
55. Mulligan SJ, Davison I, Delaney KR. Mitral cell presynaptic Ca(2+) influx and synaptic transmission in frog amygdala. Neuroscience 2001; 104:137-151.
56. Peterlin ZA, Kozloski J, Mao BQ et al. Optical probing of neuronal circuits with calcium indicators. Proc Natl Acad Sci USA 2000; 97:3619-3624.
57. Mao BQ, Hamzei-Sichani F, Aronov D et al. Dynamics of spontaneous activity in neocortical slices. Neuron 2001; 32:883-898.
58. Smetters D, Majewska A, Yuste R. Detecting action potentials in neuronal populations with calcium imaging. Methods 1999; 18:215-221.
59. Regehr WG, Tank DW. Selective fura-2 loading of presynaptic terminals and nerve cell processes by local perfusion in mammalian brain slice. J Neurosci Methods 1991; 37:111-119.
60. Atluri PP, Regehr WG. Determinants of the time course of facilitation at the granule cell to Purkinje cell synapse. J Neurosci 1996; 16:5661-5671.
61. Dittman JS, Regehr WG. Contributions of calcium-dependent and calcium-independent mechanisms to presynaptic inhibition at a cerebellar synapse. J Neurosci 1996; 16:1623-1633.
62. Chen C, Regehr WG. The mechanism of cAMP-mediated enhancement at a cerebellar synapse. J Neurosci 1997; 17:8687-8694.
63. Sabatini BL, Regehr WG. Timing of neurotransmission at fast synapses in the mammalian brain. Nature 1996; 384:170-172.
64. Sabatini BL, Regehr WG. Control of neurotransmitter release by presynaptic waveform at the granule cell to purkinje cell synapse. J Neurosci 1997; 17:3425-3435.

65. Wu LG, Saggau P. Pharmacological identification of two types of presynaptic voltage- dependent calcium channels at CA3-CA1 synapses of the hippocampus. J Neurosci 1994; 14:5613-5622.
66. Wu LG, Saggau P. Adenosine inhibits evoked synaptic transmission primarily by reducing presynaptic calcium influx in area CA1 of hippocampus. Neuron 1994; 12:1139-1148.
67. Wu LG, Saggau P. Presynaptic calcium is increased during normal synaptic transmission and paired-pulse facilitation, but not in long-term potentiation in area CA1 of hippocampus. J Neurosci 1994; 14:645-654.
68. Parri HR, Gould TM, Crunelli V. Spontaneous astrocytic Ca^{2+} oscillations in situ drive NMDAR-mediated neuronal excitation. Nat Neurosci 2001; 4:803-812.
69. Kang J, Jiang L, Goldman SA et al. Astrocyte-mediated potentiation of inhibitory synaptic transmission. Nat Neurosci 1998; 1:683-692.
70. Scanlon M, Williams DA, Fay FS. A Ca^{2+}-insensitive form of fura-2 associated with polymorphonuclear leukocytes. Assessment and accurate Ca^{2+} measurement. J Biol Chem 1987; 262:6308-6312.
71. Williams DA, Fay FS. Intracellular calibration of the fluorescent calcium indicator Fura-2. Cell Calcium 1990; 11:75-83.
72. Moore ED, Becker PL, Fogarty KE et al. Ca^{2+} imaging in single living cells: theoretical and practical issues. Cell Calcium 1990; 11:157-179.
73. Blatter LA, Wier WG. Intracellular diffusion, binding, and compartmentalization of the fluorescent calcium indicators indo-1 and fura-2. Biophys J 1990; 58:1491-1499.
74. Homolya L, Hollo Z, Germann UA et al. Fluorescent cellular indicators are extruded by the multidrug resistance protein. J Biol Chem 1993; 268:21493-21496.
75. Konishi M, Olson A, Hollingworth S et al. Myoplasmic binding of fura-2 investigated by steady-state fluorescence and absorbance measurements. Biophys J 1988; 54:1089-1104.
76. Poenie M. Alteration of intracellular Fura-2 fluorescence by viscosity: A simple correction. Cell Calcium 1990; 11:85-91.
77. Yuste R, Majewska A, Cash SS et al. Mechanisms of calcium influx into hippocampal spines: heterogeneity among spines, coincidence detection by NMDA receptors, and optical quantal analysis. J Neurosci 1999; 19:1976-1987.
78. Nett WJ, Oloff SH, McCarthy KD. Hippocampal astrocytes in situ exhibit calcium oscillations that occur independent of neuronal activity. J Neurophysiol 2002; 87:528-537.
79. Holthoff K, Tsay D, Yuste R. Calcium dynamics of spines depend on their dendritic location. Neuron 2002; 33:425-437.
80. Carter AG, Regehr WG. Prolonged synaptic currents and glutamate spillover at the parallel fiber to stellate cell synapse. J Neurosci 2000; 20:4423-4434.
81. Helmchen F, Borst JG, Sakmann B. Calcium dynamics associated with a single action potential in a CNS presynaptic terminal. Biophys J 1997; 72:1458-1471.
82. Basarsky TA, Duffy SN, Andrew RD et al. Imaging spreading depression and associated intracellular calcium waves in brain slices. J Neurosci 1998; 18:7189-7199.
83. Grondahl TO, Hablitz JJ, Langmoen IA. Depletion of intracellular Ca^{2+} stores or lowering extracellular calcium alters intracellular Ca^{2+} changes during cerebral energy deprivation. Brain Res 1998; 796:125-131.
84. Grondahl T, Langmoen IA. Confocal laser scanning microscopy used to monitor intracellular Ca^{2+} changes in hippocampal CA 1 neurons during energy deprivation. Brain Res 1998; 785:58-65.
85. Feller MB, Delaney KR, Tank DW. Presynaptic calcium dynamics at the frog retinotectal synapse. J Neurophysiol 1996; 76:381-400.

http://www.springer.com/978-0-306-47840-6

Voltage-Gated Calcium Channels
Zamponi, G.W. (Ed.)
2005, XIV, 378 p. 103 illus., 6 illus. in color., Hardcover
ISBN: 978-0-306-47840-6